Geochemistry Geophysics Geosystems G3

Published by AGU and the Geochemical Society

Article
Volume 13, Number 1
28 March 2012
Q03022, doi:10.1029/2011GC003966
ISSN: 1525-2027

Anisotropy of magnetic susceptibility of the Jingou River section: Implications for late Cenozoic uplift of the Tian Shan

Zihua Tang
Key Laboratory of Cenozoic Geology and Environment, Institute of Geology and Geophysics, Chinese Academy of Sciences, Beijing 100029, China (tangzihua@mail.iggcas.ac.cn)

Also at MOE Key Laboratory of Western China's Environmental System, Lanzhou University, Lanzhou 730000, China

Baochun Huang
State Key Laboratory of Lithospheric Evolution, Institute of Geology and Geophysics, Chinese Academy of Sciences, Beijing 100029, China

Xinxin Dong
Key Laboratory of Cenozoic Geology and Environment, Institute of Geology and Geophysics, Chinese Academy of Sciences, Beijing 100029, China

Junliang Ji
Key Laboratory of Biogeology and Environmental Geology of Ministry of Education, China University of Geosciences, Wuhan 430074, China

Zhongli Ding
Key Laboratory of Cenozoic Geology and Environment, Institute of Geology and Geophysics, Chinese Academy of Sciences, Beijing 100029, China

[1] Better constraints on the uplift history of Tian Shan will increase our understanding of both mountain building processes and deformation patterns related to the India-Asian collision. Anisotropy of magnetic susceptibility (AMS) holds great potential to track variations in tectonic strain, which is ultimately responsible for mountain uplift. Here we present an AMS record, spanning the interval of 28–4 Ma, from the fluviolucastrine Jingou River section in the Tian Shan foreland. Rock magnetic measurements show that the AMS are dominated by antiferromagnetic hematite and some paramagnetic minerals, both of which have a crystallographic preferred orientation, and therefore the AMS sequence may be applied to reconstruct tectonic strain. Although the principal minimum (K_{min}) direction is nearly perpendicular to the bedding plane, indicative of a predominantly sedimentary fabric for the section, the tightly grouped principal maximum (K_{max}) parallel to the fold axis suggests that the section was subject to an embryonic deformation at least since the Late Oligocene. The K_{max} direction is most likely associated with the N-S strain caused by the India-Asian collision. During the intervals of 23.3–20.0 Ma and 16.5–14.0 Ma, the strain markedly increased as evidenced by more tightly grouped K_{max} directions and K_{min} largely distributed within a clear N–S girdle. These two intervals are accompanied by changes in sedimentary facies (higher energy conditions and doubled sedimentation rates), and are interpreted as the periods when the Tian Shan experienced significant uplift. A conceptual model is tentatively proposed to reconcile various timings for the Tian Shan uplift.

Components: 8000 words, 9 figures.

Keywords: Tian Shan; anisotropy of magnetic susceptibility; magnetic fabrics; rock magnetism; tectonic uplift.

Index Terms: 1518 Geomagnetism and Paleomagnetism: Magnetic fabrics and anisotropy; 1525 Geomagnetism and Paleomagnetism: Paleomagnetism applied to tectonics: regional, global; 1540 Geomagnetism and Paleomagnetism: Rock and mineral magnetism.

Received 17 November 2011; **Revised** 20 February 2012; **Accepted** 20 February 2012; **Published** 28 March 2012.

Tang, Z., B. Huang, X. Dong, J. Ji, and Z. Ding (2012), Anisotropy of magnetic susceptibility of the Jingou River section: Implications for late Cenozoic uplift of the Tian Shan, *Geochem. Geophys. Geosyst.*, *13*, Q03022, doi:10.1029/2011GC003966.

1. Introduction

[2] Late Cenozoic Tian Shan uplift directly results from the India-Asian collision (Figure 1a). Determining the processes that control mountain building will provide a framework for understanding intracontinental crustal deformation, constrain the timing and rate of strain propagation due to the collision, and test the causal relationship between development of the Tian Shan and the collision.

[3] During past decades, multidisciplinary researchers have proposed various uplift histories for the Tian Shan. It is generally accepted, for example, that the major episode of uplift occurred during the middle to late Cenozoic; however, its precise age ranges from late Oligocene [*Windley et al.*, 1990; *Hendrix et al.*, 1994; *Yin et al.*, 1998; *Heermance et al.*, 2007] to mid- or late Miocene [*Bullen et al.*, 2001; *Charreau et al.*, 2006, 2009a; *Huang et al.*, 2006; *Sun and Zhang*, 2009; *Sun et al.*, 2009], and even into the Quaternary [*Burchfiel et al.*, 1999; *Chen et al.*, 2002; *Fu et al.*, 2003]. These results mainly came from the consequences of mountain uplift, while changes in tectonic strain, which essentially cause mountain building, are largely ignored.

[4] Tectonic strain could be traced by various proxies in foreland sediments. Among them, anisotropy of low-field magnetic susceptibility (AMS) analysis is a rapid and sensitive technique for measuring preferred orientations of magnetic grains and, therefore holds great potential for acquiring fabric information. AMS associates the linear relationship between an applied magnetic field (H) and the induced magnetization (M), and is defined by a symmetric second-order tensor, [K], that is given by $M = [K]H$ and has six independent matrix elements. The eigenvectors and eigenvalues of [K], $K_{max} \geq K_{int} \geq K_{min}$, give the orientations and lengths of the three principal axes of the magnetic anisotropy ellipsoid. The AMS ellipsoid is spherical when $K_{max} \approx K_{int} \approx K_{min}$, oblate when $K_{max} \approx K_{int} \geq K_{min}$, prolate when $K_{max} \geq K_{int} \approx K_{min}$, and triaxial if $K_{max} > K_{int} > K_{min}$ [*Hrouda*, 1982; *Tauxe*, 2005]. Considerable research has shown links between preferred orientations of mineral grains, the AMS ellipsoid, and strain [*Borradaile and Henry*, 1997; *Borradaile*, 2001; *Soto et al.*, 2009], even in foreland basins where strata generally are only weakly deformed with subtle tectonic fabrics [*Parés*, 2004; *Huang et al.*, 2006].

[5] Here we present a long-term AMS record from the northern Tian Shan to reconstruct tectonic stress history during the late Cenozoic and, together with sedimentary records, to further constrain the timing of the mountain building.

2. Geological Setting

[6] The Tian Shan may be tracked back to a late Paleozoic fold belt and probably remained higher than its surrounding region throughout the Mesozoic and Cenozoic times [*Windley et al.*, 1990; *Hendrix et al.*, 1992]. Subsequent erosion shed from the ancestral Tian Shan deposited thick clastic sediments in adjacent basins. To the north, approximately 10 km of terrigenous sediments accumulated in the Junggar Basin as it evolved during the Mesozoic and Cenozoic eras, of which 7 km are assigned to the Cenozoic [*Xinjiang Institute of Geography*, 1986]. Late Cenozoic reactivation of the late Paleozoic folds results in the modern topography of the Tian Shan and deforms the sediment on its piedmonts, resulting in three successive fold-thrust belts in the southern margin of the Junggar Basin (Figure 1b). The fold-thrust belts were incised by north-flowing rivers and exposed the late Mesozoic to Cenozoic strata. Close to the

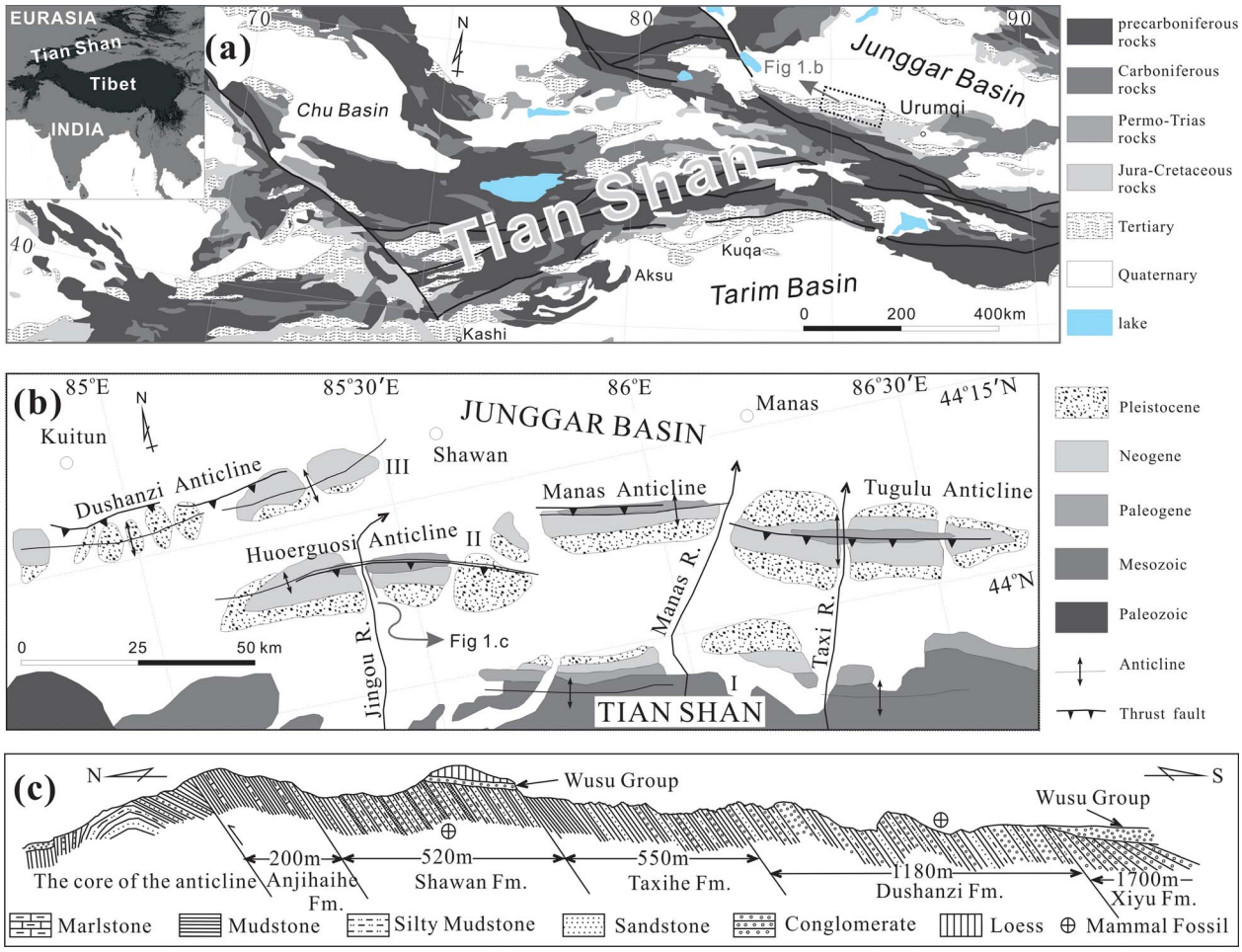

Figure 1. (a) Geological sketch map of the Tian Shan Range. Inset shows topography of the Tibetan Plateau and the Tian Shan. (b) Geological map of the study area showing the threefold-thrust zones (I, II, and III) and the location of the Jingou River section. (c) Strata exposed at the Jingou River section. Note the growth strata Xiyu Formation.

Tertiary depocenter within the basin, the Jingou River incises the Huoerguosi Anticline in the central fold-thrust to expose a continuous section of south dipping sediments sampled for our work.

[7] The Jingou River section (44°10.4′N, 85°27.4′E) comprises, in ascending order, the Anjihaihe, Shawan, Taxihe, Dushanzi and Xiyu Formations with no significant hiatuses [*Li*, 1984]. All these formations are well exposed in the southern limb of the Huoerguosi Anticline along the Jingou River valley (Figure 1c). The Anjihaihe Formation, cropping out in the northernmost part of the section, is mainly composed of grayish green mudstone with parallel laminations and is interpreted to represent lake facies, implying a distal source sediment in a large low-relief basin. To the south, the overlying Shawan Formation is lithologically divided into three units. The low unit, ~100 m thick, is dominated by dark brown massive mudstones, the middle unit is made up of ≥18 couplets of red-brown silty mudstone and conglomerates with a thickness of ~250 m, and the upper unit consists of brown and slightly grayish green silty mudstones. These are interpreted as a lacustrine prodelta, distal fan-delta, and delta front facies, respectively. The Taxihe Formation contains green sandstones intercalated with brown mudstones to siltstones toward its base and brown silty mudstones to sandstones toward the top, indicative of lacustrine and fluvial delta plain facies, respectively. The upper part of a fluvial delta plain facies is ~450 m thick and gradually coarsens upwards. The overlying Dushanzi Formation consists mainly of brown pebbly sandstones, conglomerates and interbedded silty mudstones, representing a braided river and alluvial fan facies. The Dushanzi Formation grades into the overlying

Xiyu Formation within 200 m of strata dominated by conglomerates and subordinate fine grained sandstones. The Xiyu Formation is characterized by dark gray conglomerates with rare lenses of siltstones and sandstones in the lower part, and is interpreted as a debris-flow fan facies. From the base of the Xiyu Formation upwards, growth strata are developed and unconformably overlain by the Pleistocene Wusu Group.

[8] The chronology of the Jingou River section is based on biostratigraphic age control and high resolution magnetostratigraphy [*Tang et al.*, 2011], and is consistent with previous results [*Charreau et al.*, 2009b] for the same valley. This work yields a basal age of ~28 Ma for the sampled section and 7 Ma for the base of the Xiyu Formation, i.e., the initiation of the growth strata.

3. Materials and Methods

[9] AMS sampling was designed to yield a temporal resolution of ~50 ka with 562 samples collected. At each site, the finest grain-size at the outcrop scale and horizons without paleocurrent indicators in the case of sandstones were chosen for sampling to minimize the impacts of transport induced anisotropy. The sample ages are assigned by linear interpolation of paleomagnetic reversals [*Tang et al.*, 2011].

[10] Rock magnetic measurements were carried out. The contributions of ferromagnetic and paramagnetic mineral phases to AMS were determined for the selected samples distributed along the section. Experiments include temperature dependence of magnetic susceptibility (*k*-T curves), acquisition and backfield demagnetization of isothermal remanent magnetization (IRM), and measurement of hysteresis properties. Thermomagnetic analysis was performed using a KLY-3S Kappabridge with a CS-3 high-temperature furnace. Hysteresis loops, as well as IRM curves, were measured on a variable field translation balance (VFTB) at the Institute of Geology and Geophysics (IGG), Chinese Academy of Sciences (CAS), with the maximal applied magnetic field 1 T. Hysteresis loops have been corrected for paramagnetism and mass normalized.

[11] The AMS was measured with an AGICO KLY-3S Kappabridge susceptibility meter at the IGG, CAS, which operates at 300 A/m at a frequency of 875 Hz and has a typical sensitivity of $\sim 2.0 \times 10^{-8}$ SI. The corrected anisotropy degree (P_j), and shape parameter (T), defined by *Jelinek* [1981], were calculated.

4. Results

4.1. Magnetic Mineralogy

[12] Thermomagnetic investigation (*k*-T curves) and acquisition and backfield demagnetization of isothermal remanent magnetization (IRM) experiments were performed to characterize the magnetic mineralogy. The *k*-T curves show a significant decrease in magnetic susceptibility in all measured samples in the 500–580°C range [*Petrovský and Kapička*, 2006] (Figure 2), indicating the presence of magnetite. This decrease is more pronounced in the upper part of the section than in the lower part, which may indicate greater magnetite abundance in the upper section. IRM increases rapidly in fields <0.3 T, consistent with the presence of magnetite. However, the low values (0.15–1.5 μAm^2) for the saturation magnetic moment (Figure 6a) indicate limited magnetite in the Jingou River section. The IRM curves also suggest that the samples contain a mineral that is not saturated by a field ~1 T, which, together with unblocking temperatures above 600°C identified from thermal demagnetization curves for most samples [*Ji et al.*, 2008], is characteristic of hematite. As shown on the back field curves, the samples from the lower part of the section have higher coercivity of remanence (Bcr) while those from the upper part have lower Bcr values. Samples from the upper section show Bcr values close to the theoretical SD magnetite Bcr for equidimensional grains (33 mT [*Dunlop and Özdemir*, 2001]), suggesting that fine-grained magnetite is present. Much higher Bcr of the other samples suggests the combined presence of higher coercivity mineral such as hematite and goethite, agreeable with the thermomagnetic results.

[13] Hysteresis loops for the alluvial and fluvial samples approach saturation at an applied field of ~1 T and have "wasp-waisted" hysteresis loops (Figure 3a), which indicate the coexistence of at least two magnetic components, one with high coercivity and another with low coercivity [*Jackson*, 1990; *Roberts et al.*, 1995; *Tauxe et al.*, 1996], while the lacustrine samples have broader hysteresis loops indicative of higher coercivity phase. Moreover, differences in magnetic grain size between alluvial/fluvial and lacustrine samples are revealed in the Day plot [*Dunlop*, 2002] (Figure 3b). All observed alluvial/fluvial samples fall within the pseudo-single-domain (PSD) field and are relatively close to the

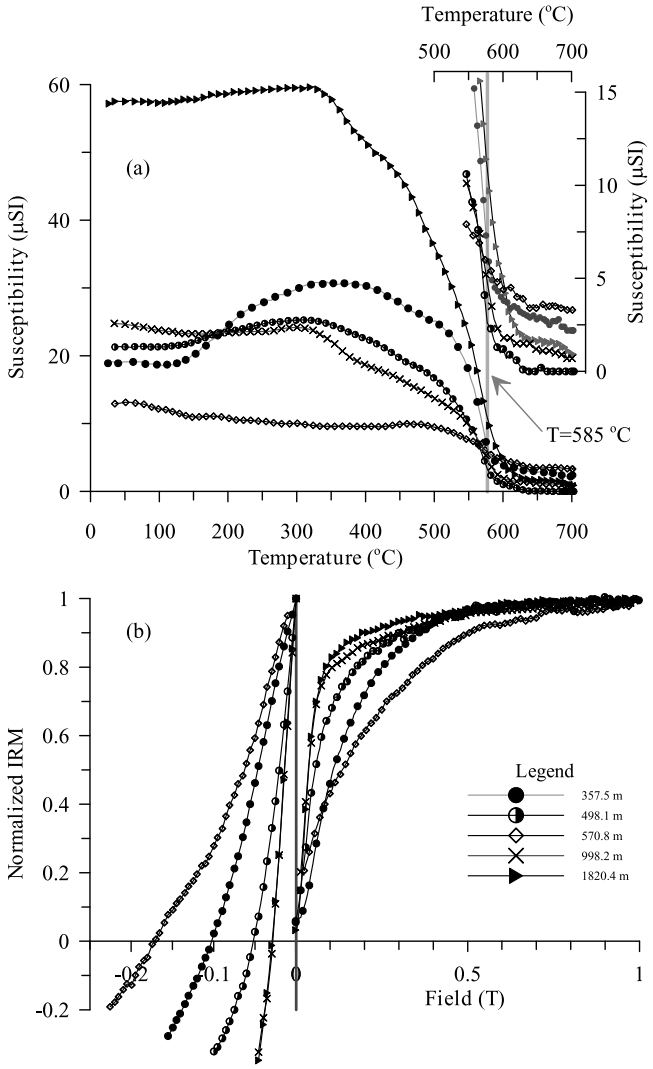

Figure 2. (a) Low-field temperature dependence of magnetic susceptibility (k–T curves) for selected samples from different level of the composite section. All spectra were measured by heating from room temperature to ~700°C in argon gas atmosphere. Inset: Enlargement of data obtained from 550 to 700°C. (b) Behavior of acquisition and back-field demagnetization of isothermal remanent magnetization (IRM) for the samples.

mixing line of single-domain (SD) and multidomain (MD) grains derived by *Dunlop* [2002]. In contrast, the lacustrine samples, largely in the SP+SD field and partially in the PSD field, are away from the mixing line, implying a larger grain size of magnetic minerals than alluvial/fluvial samples. It seems that the granulometry of magnetic minerals is somewhat decoupled from the grain size of the sediment contained the magnetic grains, suggesting complex variations in relative abundance of magnetic minerals in the Jingou River section.

4.2. Anisotropy of Magnetic Susceptibility

[14] Magnetic susceptibilities and AMS fabrics were determined for 562 specimens and show significant changes with stratigraphic position and lithology in the section (Figure 4; see Data Set S1 in the auxiliary material for original AMS data).[1] Bulk magnetic susceptibility (k_m) ranges from 26 to 1758 μSI with an average of 329 $\pm$ 259 μSI. Mean magnetic susceptibility is the lowest at the base of the section; it obviously increases at ~22 Ma (~350 m thickness) and then remains at a relatively high value to ~20 Ma (~500 m thickness). It is then followed by a 5.7 Ma interval (~22–16.3 Ma) of low values mostly below 200 μSI. At ~16.3 Ma (825 m), the k_m displays a marked increase and then progressively increases to a maximum (>600 μSI) until

[1]Auxiliary materials are available at ftp://ftp.agu.org/apend/gc/2011gc003966.

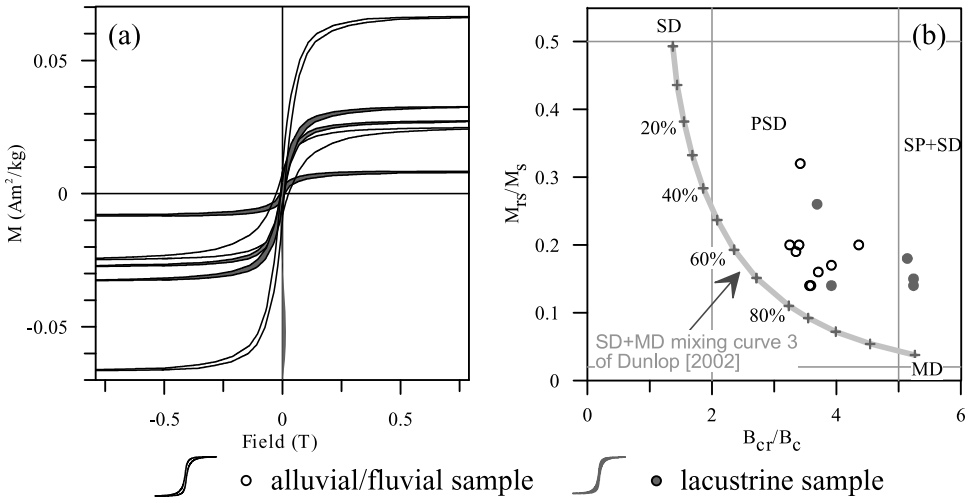

Figure 3. (a) The selected examples of slope-corrected hysteresis loops. (b) Hysteresis ratios for all data are plotted, ratio of coercivity of remanence (Bcr) to coercivity (Bc) versus ratio of saturation remanence (Mrs) to saturation magnetization (Ms) [*Dunlop*, 2002]. Thick gray line represents theoretical variation trend for mixture of single-domain (SD) and multidomain (MD) grains after curve 3 of *Dunlop* [2002].

~11 Ma (~1630 m), and remains high thereafter. At the Jingou River section, the degree of anisotropy (P_j) ranges from 1.004 to 1.083 with a mean of 1.03 and is independent of lithology. However, the shape parameter T shows significant changes. From ~28 Ma to ~23.3 Ma, the ellipsoids are oblate with a mean T value of 0.621. Subsequently, T shifts to distinctly negative values until ~20 Ma where it slowly shifts to positive values. After ~16.5 Ma, T again decreases to a trough centered at 16 Ma, then gradually rises once again, reaching 0.3 by 14 Ma; it then becomes generally oblate and slightly more oblate toward the top of the section.

[15] Stereonet projections of the K_{max} and K_{min} principal axes of the AMS ellipsoids are shown in Figure 5. The tilt-corrected K_{max} are well grouped in an approximately east-west direction, with a low inclination, and generally parallel to the fold axis, while the tilt-corrected K_{min} show a slight girdle distribution, perpendicular to the fold axis, and yield a mean direction with a slight trend to the north. These distributions of the principal anisotropy axes are commonly found in folded sediments especially from foreland basins [*Gilder et al.*, 2001; *Parés*, 2004; *Huang et al.*, 2006, 2010].

5. Interpretations

5.1. Sources of Magnetic Susceptibility and Its Anisotropy

[16] Owing to its magnetization greater than that of other magnetic minerals by two orders of magnitude, magnetite as susceptibility can be recognized in almost every thermomagnetic curve, characterized by a marked drop at temperature 500–580°C, as shown in Figure 2a. Magnetite generally dominates the magnetic behavior of sediments when present as ≥0.5% of the iron oxide fraction [*Evans and Heller*, 2003]. However, the magnetic properties of the Jingou River section are controlled by anisotropic paramagnetic and antiferromagnetic minerals, instead of magnetite. The average value for the saturation magnetic moment in the section is 0.15–1.5 μAm^2 (Figure 6a). The low values suggest a magnetite concentration of $0.1–1 \times 10^{-3\%}$ by weight [*Hrouda and Kahan*, 1991]. The corresponding volume susceptibility for this percentage of magnetite is 5 μSI, which is less than 3% of the bulk susceptibility (5 out of 231 μSI) in most samples of the study section. As evidenced from the plot of k_m versus P_j (Figure 6b), the independence of P_j to k_m, accompanied by the overall relatively low k_m, indicates the dominant control of anisotropic paramagnetic and antiferromagnetic minerals on both susceptibility and anisotropy of the sediments [*Tarling and Hrouda*, 1993]. Moreover, the elongated distribution of AMS ellipsoids (P_j-T data) does not pass through, or toward, the magnetite AMS ellipsoid (Figure 6c) and indicates that the observed AMS is not a direct function of magnetite concentration change [*Parés*, 2004]. These lines of evidence, coupled with the unblocking temperature above 600°C, suggest that hematite contributes mainly to the bulk susceptibility and its anisotropy.

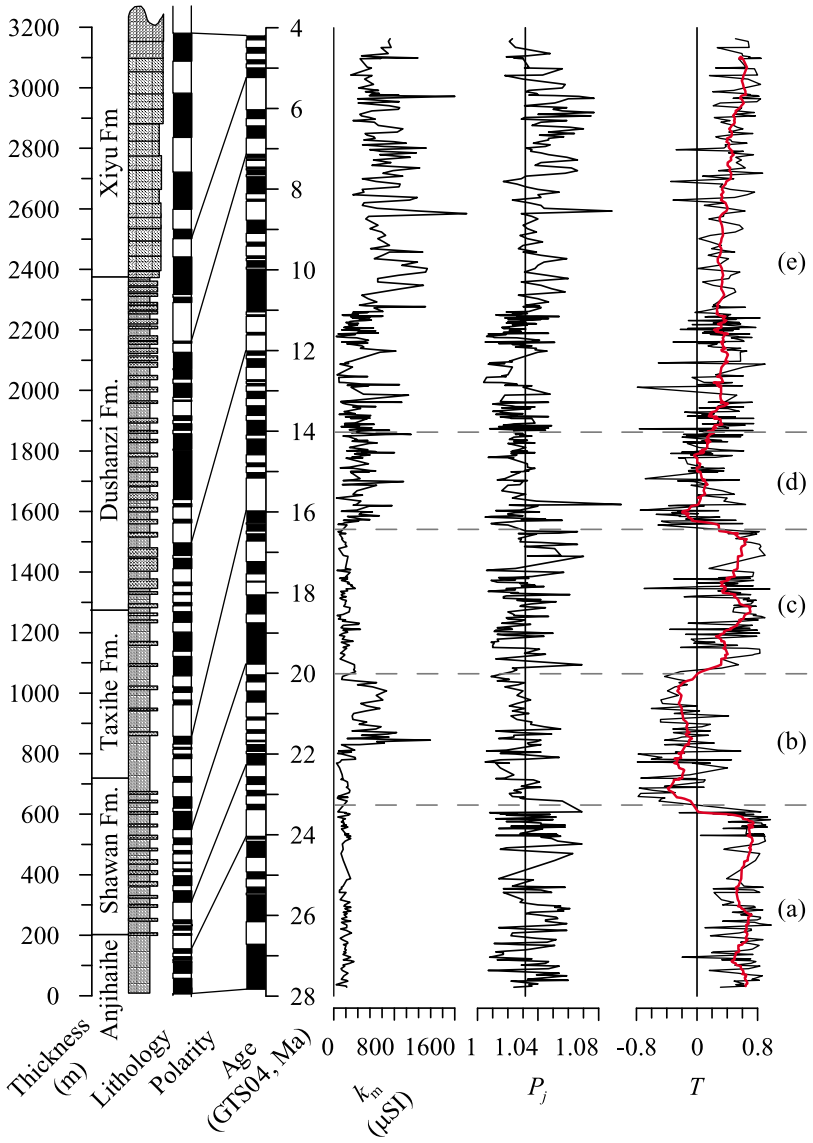

Figure 4. Synthetic lithologic column, the revised chronology for the Jingou River section correlating to the GTS04 [*Ogg and Smith*, 2004], and rock magnetic results comprising mean magnetic susceptibility (k_m), corrected AMS degree (P_j), and shape parameter (T) of the AMS ellipsoids shown as a function of age.

[17] If hematite is the primary mineral influencing the AMS fabric, then the origin of this hematite must be explained carefully. The type and timing of the remanence acquisition in these sediments remains controversial. In the Jingou River section, the same directions of the NRM carried by the medium-temperature (360–580°C) component and the high-temperature hematite component (>600°C) (see *Ji et al.* [2008, Figure 5] and *Charreau et al.* [2009b, Figure 5] for details) suggest that there is no detectable delay in NRM acquisition between the medium and the high-temperature components. These common directions, coupled with the bedding perpendicular directions of the K_{min} (Figure 5), suggest that the hematite-carried remanence is most likely primary, independent of the type of the remanence acquisition.

[18] These results suggest that the AMS of the Jingou River section expresses a crystallographic preferred orientation for hematite, instead of a shape preferred orientation for magnetite. Thus, the AMS sequence from the Jingou River section holds

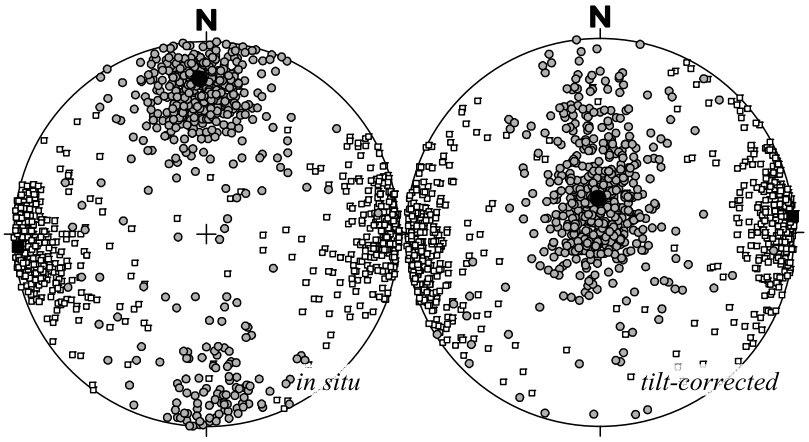

Figure 5. Equal-area stereographic projections of AMS principal axes in specimen (in situ) and bedding (tilt-corrected) coordinate to show primary sedimentary fabrics preserved in the section characterized by the bedding perpendicular K_{min} directions. Squares and circles show orientations of K_{max} and K_{min} axes, respectively, and the solid squares and circles represent their means.

potentials to track paleostrain related to tectonic processes.

5.2. Strain Evolution Indicated by AMS Record and Implications for the Tian Shan Uplift

[19] Numerous studies have speculated that changes in magnetic fabrics can capture the earliest stage of deformation that occurred shortly after deposition and prior to lithification of the rocks, even where microscopic evidence of deformation is not visible [e.g., *Kligfield et al.*, 1983; *Cifelli et al.*, 2004; *Burmeister et al.*, 2009]. Most recently published AMS data from Holocene sediments recovered in Lake Ussyk-Kul in the Kyrgyz Tien Shan, ~700 km west of our section, further indicates that tectonic fabric can be found in sediments as young as 25-yr-old, and locked within sediments older than 1180 yr before present [*Larrasoaña et al.*, 2011]. The delay of AMS response to tectonic strain is instantaneous in the context of geologic time and thus we interpret our AMS record as a sensitive proxy for tectonic strain.

[20] Theoretical and field data show that an idealized suite of AMS ellipsoids develops in fold-thrust belts as primary sedimentary fabrics are progressively overprinted by tectonic fabrics [*Borradaile and Tarling*, 1981; *Parés and van der Pluijm*, 2002; *Parés*, 2004; *Weil and Yonkee*, 2009]. In an undeformed condition, primary sedimentary fabrics are controlled by depositional and diagenetic processes and are characterized by oblate AMS ellipsoids with $K_{max} \approx K_{int}$ within the bedding plane and K_{min} perpendicular to bedding. During

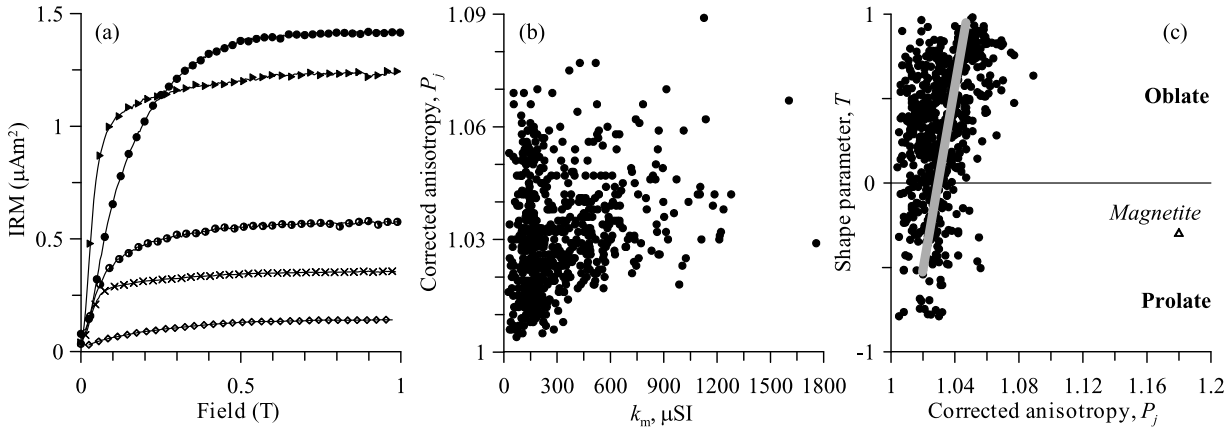

Figure 6. (a) Acquisition of saturation magnetic moment for the samples shown in Figure 2. (b) Mean magnetic susceptibility (k_m) versus corrected anisotropy (P_j). (c) P_j–T diagram of the Jingou River section. The AMS ellipsoid for magnetite (P_j = 1.18, T = −0.30 [*Tarling and Hrouda*, 1993]) is shown by the triangle.

the embryonic deformation with weak layer-parallel strain, K_{max} clusters toward a direction perpendicular to the internal strain direction while K_{min} remains perpendicular to the bedding. The AMS ellipsoid correspondingly becomes triaxial. If the strain progressively increases and moderate deformation is developed, K_{max} strongly clusters perpendicular to the strain, K_{min} begins to scatter away from the bedding pole, forming a girdle along the strain direction, and the AMS ellipsoid becomes prolate [*Parés*, 2004]. For a higher strain that leads to strong deformation in strata, the tectonic fabrics overprint the sedimentary fabrics, K_{min} clusters parallel to the strain and K_{max} gradually clusters to the bedding pole. Moreover, a general P_j-T path [*Borradaile and Henry*, 1997; *Parés*, 2004] describes the evolution of AMS ellipsoids as the intensity of deformation increases. In response to increasing infinite strain, the AMS ellipsoid shifts from oblate to prolate with a significant decrease in T and a slight decline in P_j in weakly deformed rocks.

[21] Since the Mesozoic, sediments shed from the Tian Shan are transported by north-flowing hydrologic systems like the Jingou River [*Hendrix et al.*, 1992]. If the primary sedimentary fabrics are well preserved in the AMS record, the K_{max} striking N–S direction and K_{min} perpendicular to bedding with slight tilt to north should be expected. From the tilt-corrected stereographic projection (Figure 5), K_{min} approximately perpendicular to the bedding is as the excepted, and the observed K_{max} direction of the overall section is near E–W and parallel to the axis of the Huoerguosi Anticline, unequivocally showing the sustained presence of strain in a N–S direction and a slight to moderate overprint of tectonic fabric by the primary sedimentary fabrics over the 28–4.2 Ma interval. Rocks partially affected by weak deformation resulting from N–S directed compression have been reported in the sedimentary succession north of the Tibetan Plateau, in the Subei region of the Qaidam Basin [*Gilder et al.*, 2001], and the Kuche Depression of the Tarim Basin [*Charreau et al.*, 2006; *Huang et al.*, 2006]. All of these examples have been attributed to the strain propagated from the India–Asian collision, which initiated during the early Cenozoic [e.g., *Najman et al.*, 2010; *Chen et al.*, 2010; *Yi et al.*, 2011].

[22] To track possible changes in the strain, we further divided the section into five portions (Figure 7). From the base to the thickness of 200 m in the section (Figure 7a, 28.0–23.3 Ma), the K_{min} still grouped around the bedding pole while K_{max} is near parallel to the fold axes, showing a characteristic of the initial stage of the deformation as mentioned above. For the portion between the thickness of 200 to 520 m (Figure 7b, 23.3–20.0 Ma), K_{max} remains parallel to the fold axes and becomes more tightly grouped and K_{min} is largely distributed within a clear N–S girdle. This is a reflection of an increased strain during the interval. The increased strain is further supported by the decreasing value of the ellipsoid shape parameter T, as shown in Figure 4. Between the levels of 520–∼810 m (Figure 7c, 20–16.5 Ma), the K_{max} shows a greater scatter although little changes in its mean direction, the K_{min} clustered around the bedding pole. These distributions of the principal anisotropy axes duplicate the pattern of the 28–23.3 Ma interval and subsequently the AMS ellipsoid shape return to be oblate ($T > 0$), suggesting an embryonic deformation by a weak strain. At the thickness of 820–1150 m (Figure 7d, 16.5–14.0 Ma), K_{min} axes are distributed in a near N–S girdle, K_{max} is tightly clustered along the fold axis again, collectively indicating a relatively moderate deformation due to the N-S direction of compression. At ∼16.5 Ma, T correspondingly decreases to 0 by 14 Ma, signifying a stage of increased strain. Above this level (Figure 7e, 14.0–∼4 Ma), AMS ellipsoids are characterized by more dispersed K_{max} distributions with constant mean direction parallel to the fold axis and K_{min} grouped around the bedding pole, displaying an initial modification of weak strain to the primary sedimentary fabrics.

[23] The episodic increase of the strain derived from the principal anisotropy axes is also reflected by the shape parameter (T). According to the empirical and theoretical P_j–T path, the AMS ellipsoid shape of a weakly deformed region, such as foreland basins where the Jingou River section located, is featured by a trend from oblate ($T > 0$) to prolate ($T < 0$) with increasing strain. In the Jingou River section, the ellipsoid shapes were dominantly oblate during the late Oligocene and shifted to predominantly prolate around ∼23.3 Ma. The ellipsoids remained prolate until 20 Ma and subsequently changed to oblate till ∼16.5 Ma. From ∼16.5 Ma to 14 Ma, the ellipsoids then became prolate or triaxial and finally regained their oblateness at ∼14.0 Ma. Clearly, the two periods of increased strain correlate precisely to those recorded by the principal axes, i.e., 23.3–20.0 Ma and 16.5–14.0 Ma, respectively.

[24] The observed AMS fabrics incorporate an invisible, but magnetically detectable, signature of the persistent tectonic strain that increased

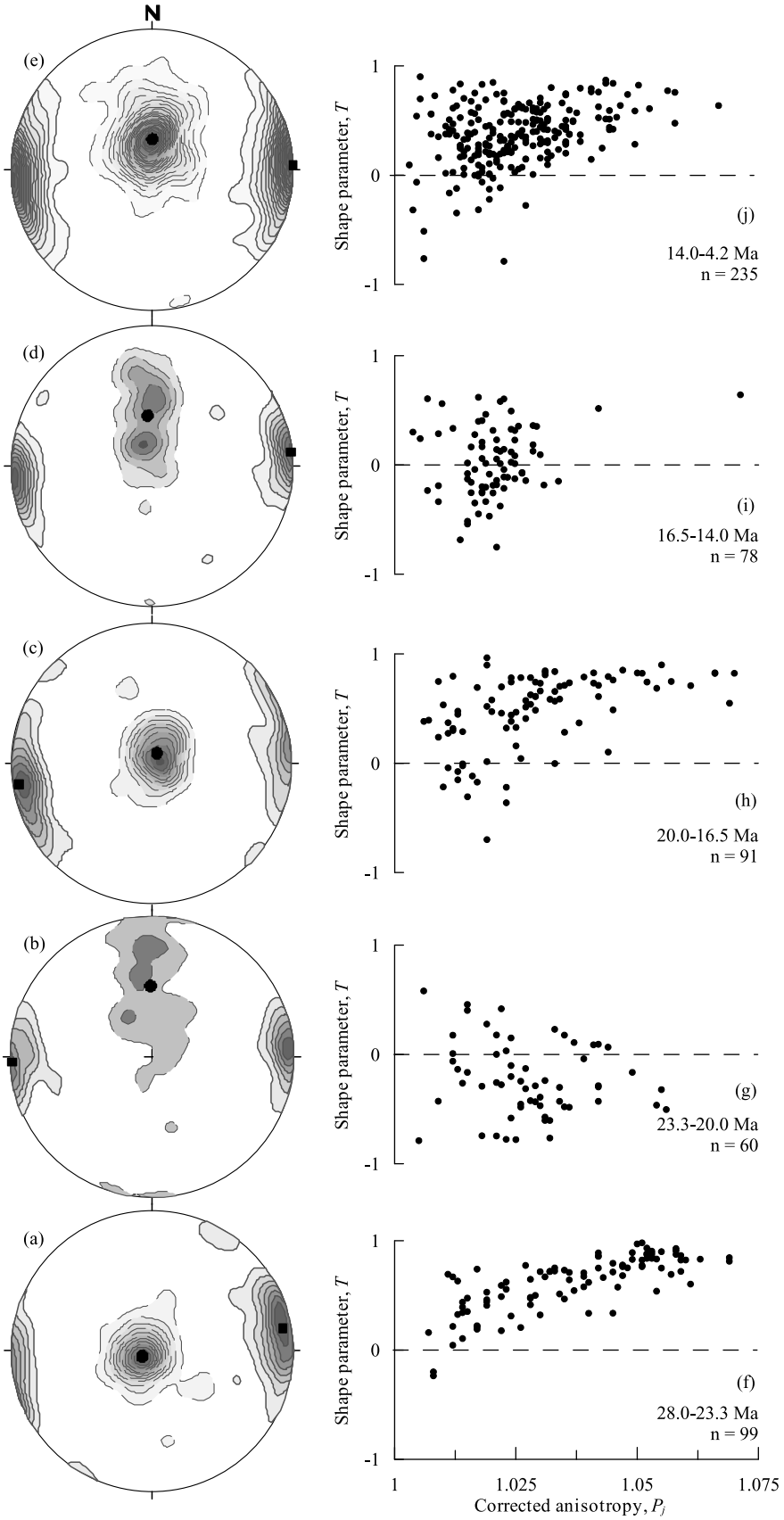
N
(e)
(d)
(c)
(b)
(a)
Shape parameter, T
1
0
-1
(j)
14.0-4.2 Ma
n = 235
(i)
16.5-14.0 Ma
n = 78
(h)
20.0-16.5 Ma
n = 91
(g)
23.3-20.0 Ma
n = 60
(f)
28.0-23.3 Ma
n = 99
1
1.025
1.05
1.075
Corrected anisotropy, P_j

Figure 7

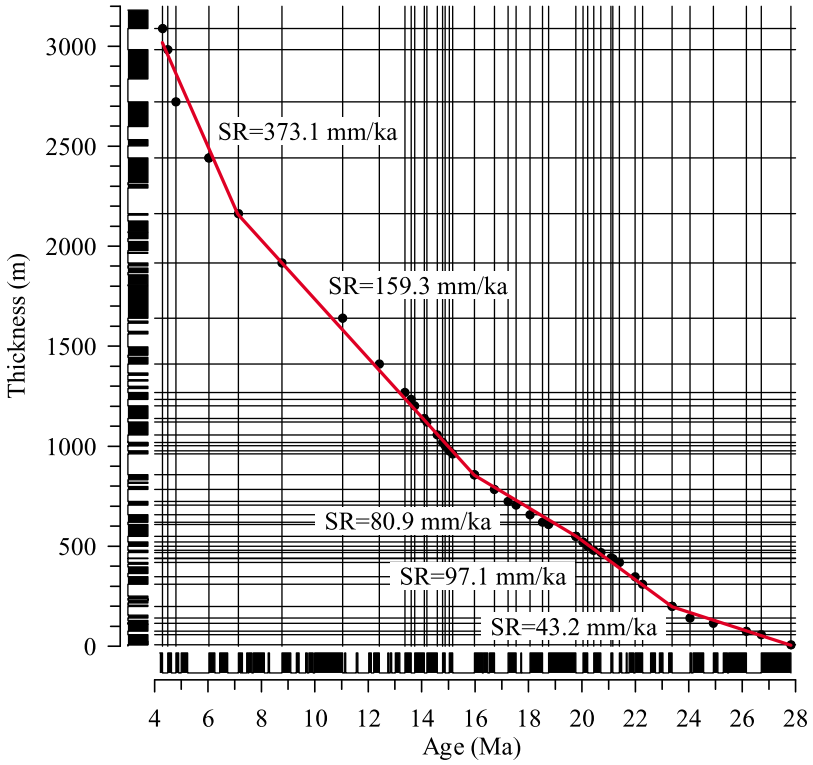

Figure 8. Age versus thickness of the Jingou River section. Age constraints are determined by the polarity chrons shown in Figure 4. The marked accelerations of the sedimentation rate occur around ~23.3, ~16 Ma and ~7 Ma.

significantly during the Early Miocene and late Middle Miocene. The late Cenozoic sedimentary infill in foreland basins is a direct response to thrusting and loading of the crust during deformation and provides an invaluable orogenic signature. Comparing the strain history with changes in sedimentary facies of the section, we can further constrain the Tian Shan uplift during late Cenozoic. According to magnetostratigraphic results [*Tang et al.*, 2011], at ~23.3 Ma, the lacustrine Anjihaihe Formation shifts quickly to the deltaic (pro- and distal fan-delta) Shawan Formation. The Anjihaihe Formation is characterized by grayish green, fine-grained sediments commonly with parallel laminations, suggesting a quiescent depositional condition. The overlying Shawan Formation is mainly comprised of red, laminated or rippled, medium to coarse-grained sandstones intercalated with pebble conglomerates, signifying a high-energy hydrodynamic regime. At ~16.5 Ma, the Jingou River section experienced a gradual transition from the lower to upper Taxihe Formation, a transition from a typical lacustrine depositional environment to a fluvial delta plain facies. The transitional stage continues to the top of the Taxihe Formation at ~1270 m thickness (~13.5 Ma) and is marked by the disappearance of the green lacustrine silty marls. Transitions toward higher energy depositional systems coincide with the periods of increased strain derived from the AMS records.

[25] This coincidence may be interpreted by the following mechanism. An increased tectonic strain derived from the India-Asia collision uplifts the Tian Shan, enhancing the potential energy in the hydrodynamic systems in the uplifting mountains. As a result, we might expect the sedimentation rate to be increased as a direct response to the accelerated erosion.

[26] Based on our magnetostratigraphic data, the sedimentation rate in the Jingou River was almost doubled at ~23.3 and ~16.0 Ma, respectively (Figure 8). The duration and consistency of the enhanced sedimentation rates imply that this is

Figure 7. (a–e) Density contour diagrams of AMS principal maximum (square) and minimum (circle) directions in equal-area stereographic projections for the five portions (corresponds to zones a–e in the Figure 4). The data is tile corrected. The mean direction of K_{max} and K_{min} (black square and circle, respectively) is calculated by an eigenvalue method [*Woodcock*, 1977]. (f–j) P_j-T (corrected AMS degree versus AMS shape parameter) diagrams for AMS data for the five portions from the Jingou River section.

most likely a result of tectonic uplift [*Willett and Brandon*, 2002], instead of climate change. These independent lines of evidence, together with the AMS records, suggest that the Tian Shan experienced, at least, two pulses of uplift at 23.3–20.0 Ma and 16.5–14.0 Ma during the late Cenozoic, as suggested from the foreland basins in the southern piedmont of this mountain range [e.g., *Yin et al.*, 1998; *Huang et al.*, 2006].

6. Discussion

[27] Evidence for late Cenozoic reactivation of the Tian Shan includes rapid cooling events based on thermochronology [*Hendrix et al.*, 1994; *Dumitru et al.*, 2001; *Du and Wang*, 2007], acceleration of sedimentation rates [*Huang et al.*, 2006; *Heermance et al.*, 2007; *Charreau et al.*, 2009b], changes in lithology [*Windley et al.*, 1990; *Yin et al.*, 1998], initiation of syntectonic growth strata [*Huang et al.*, 2010; *Sun and Zhang*, 2009; *Sun et al.*, 2009], mass balanced reconstruction [*Métivier and Gaudemer*, 1997] and the estimations using the GPS data [*Abdrakhmatov et al.*, 1996; *Reigber et al.*, 2001] and flexural modeling [*Yang and Liu*, 2002]. These results greatly improved our knowledge of intracontinental deformation; however, we still know little about its exact timing: When did the mountain building initiate? How long did the processes last? And, how do we reconcile the age differences of the mountain building based on various proxies?

[28] The work presented here establishes an AMS-based tectonic strain history from a well-dated fluviolacustrine section in the foreland basin of the Tian Shan. Accompanied by a facies transition to a high-energy fluvial system and significant increases in sedimentation rate (Figure 8), increases in the tectonic strain reveal two uplifting stage occurred at 23.3–20.0 Ma and 16.5–14.0 Ma. These episodes fall broadly within the range of the uplift timing proposed previously, but are significant older than the basal age of the growth strata (~7 Ma) in the study section.

[29] By reviewing previous chronological frameworks, we attribute the timing of uplift for the Tian Shan to differences in the research methods and their uncertainties. Growth strata, for example, are formed when sedimentation takes place during the growth of the fold, and can provide precise information on tectonic and depositional interaction [*Suppe et al.*, 1992; *Burbank et al.*, 1996], and its basal age has been applied to date the initial reactivation of the Tian Shan [*Sun and Zhang*, 2009; *Sun et al.*, 2009]. Due to the basin-ward propagation of tectonic deformation, however, the basal age of growth strata is time-transgressive, as found in the Southwestern Chinese Tian Shan foreland [*Chen et al.*, 2002, 2007], and therefore does not define the initial age of the mountain building. This conclusion is confirmed by independent studies on the Xiyu Formation, a diachronous prograding gravel wedge at the front of the Tian Shan [*Heermance et al.*, 2007; *Charreau et al.*, 2009a; *Huang et al.*, 2010]. Changes in erosion rates can be constrained from the cooling ages [*Reiners and Brandon*, 2006]. These thermochronological data suggest that the Tian Shan experienced rapid exhumations commenced at ~25–20 Ma [*Hendrix et al.*, 1994; *Sobel and Dumitru*, 1997; *Sobel et al.*, 2006] and in the late Miocene [*Sobel and Dumitru*, 1997; *Bullen et al.*, 2003; *Sobel et al.*, 2006]. Unfortunately, these interpreted ages depend on spatial and temporal variations in exhumation rates, topography, fluid circulation, and deep-derived heat flow, all of which may induce uncertainty and thus reduce the accuracy of the cooling and exhumation ages [*Reiners and Brandon*, 2006].

[30] Here we propose a conceptual model to describe mountain building in the Tian Shan and to explain the timing differences observed using various approaches (Figure 9). Although the Paleogene Tian Shan experienced widespread erosion, it was influenced by the tectonic strain associated with the India-Asian collision initiated in the early Cenozoic. At our study site in the foreland basin of Tian Shan, the K_{max} of the AMS ellipsoids clusters roughly perpendicular to the strain direction instead of parallel to flow direction. At time t_1, the strain increased enough to uplift the mountain, and quickly reoriented the AMS fabrics of sediments in forelands. The finite strain causes the K_{min} axes to form a girdle distribution on the stereographic projection along the strain direction, although there is no visible deformation in the strata. The uplifting mountains erode primarily coarser grain sizes, which prograde toward the basin. At t_2, these eroded materials arrive at the study site, resulting in a higher sedimentation rate. As a consequence of uplift, the increased sedimentation rate lags behind the enhancement of strain. Finally, the crustal deformation associated with the mountain building propagates outward and deforms foreland sediments. When the deformation arrives at the study site (t_3), sediments are simultaneously deposited on the deforming fold limb or active fault planes,

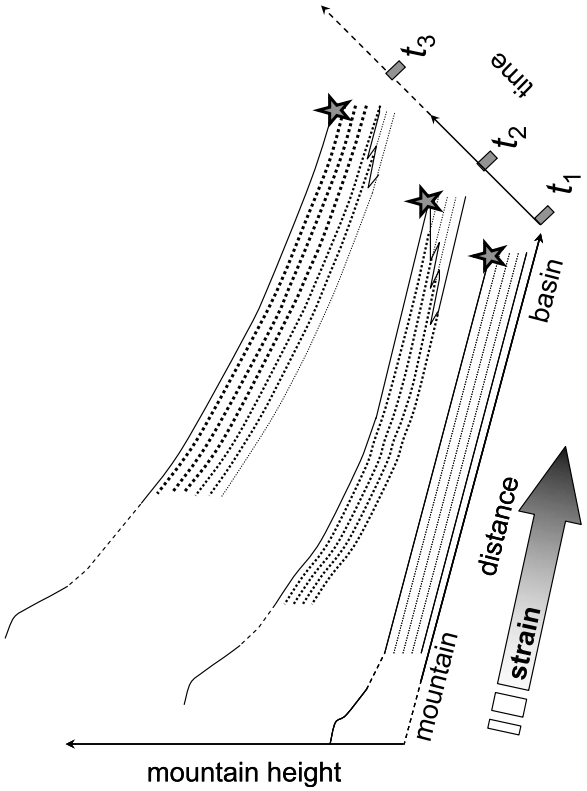

Figure 9. A conceptual model shows the timing differences of interpreted tectonic uplift in various methods. The star indicates a specific study site. t_1 represents the time of increasing strain, t_2 corresponds to the time of accelerating sedimentation rate, and t_3 correlates to the onset of the growth strata.

initiating growth strata. Since t_3, a series of progressive and syntectonic onlap angular unconformities developed, and the grain size of the sediments gradually coarsens in response to accelerated bedrock denudation.

[31] Therefore, the timing of the increased strain derived from the AMS record should be closer to the uplift timing. In contrast, the proxies based on foreland sediments, like sedimentation rates and detrital influx, may record erosion of the mountain after they have already been uplifted and transported downstream. As for growth strata, its basal age is equivalent to the initiation of fold growth and may lag far behind the mountain uplift. This lag generally increases with the distance between the erosion sources and sinks.

7. Conclusions

[32] The strain-sensitive AMS record in foreland basins reveals information about the strain history and places further constraints on mountain building. The AMS sequence from the Jingou River section of the northern Tian Shan suggests that the region was persistently under strain in N-S direction during the past 28 Ma, and the strain significantly increases during the intervals of 23.3–20.0 Ma and 16.5–14.0 Ma. The AMS-based strain measurements, together with the associated facies transitions to higher energy conditions, indicate that the Tian Shan experienced significant uplifts during the two time intervals.

[33] The current discrepancy regarding the timing of the Tian Shan uplift may result from methodological variations, and a conceptual model is presented to reconcile these differences. Mountain building results from increases in tectonic strain, and therefore, can be recorded immediately by strain-sensitive proxies, such as AMS. Later, the uplifting/uplifted mountains shed sediments basinward, leading to a higher detrital influx in the foreland, which is recorded in sedimentation rates and/or thermochronologic cooling ages. Ultimately, the foreland sediments experience the crustal deformation associated with the mountain building and the growth strata.

Acknowledgments

[34] We are indebted to the associate editor J. Feinberg and three reviewers, Michael S. Petronis, Brian O'Driscoll and Paul Kelso, whose insightful comments were implemented and greatly improved the manuscript. We are grateful to Yang Shiling, Liu Xiuming, Wang Haibin, and Liu Weiming for helpful discussions and laboratory assistance and to Jiang Hanchao, Wang Xu, and Luo Pan for sample collection. This study was supported by the Natural Science Foundation of China (grants 41102109, 40902049 and 40730208) and the Foundation of Key Laboratory of Western China's Environmental Systems (Ministry of Education) at Lanzhou University.

References

Abdrakhmatov, K. Y., S. A. Aldazhanov, B. H. Hager, M. W. Hamburger, T. A. Herring, K. B. Kalabaev, V. I. Makarov, P. Molnar, S. V. Panasyuk, and M. T. Prilepin (1996), Relatively recent construction of the Tien Shan inferred from GPS measurements of present-day crustal deformation rates, *Nature*, *384*, 450–453, doi:10.1038/384450a0.

Borradaile, G. J. (2001), Magnetic fabrics and petrofabrics: Their orientation distribution and anisotropies, *J. Struct. Geol.*, *23*, 1581–1596, doi:10.1016/S0191-8141(01)00019-0.

Borradaile, G. J., and B. Henry (1997), Tectonic applications of magnetic susceptibility and its anisotropy, *Earth Sci. Rev.*, *42*(1–2), 49–93, doi:10.1016/S0012-8252(96)00044-X.

Borradaile, G. J., and D. H. Tarling (1981), The influence of deformation mechanisms on magnetic fabrics in weakly deformed rocks, *Tectonophysics*, *77*(1–2), 151–168, doi:10.1016/0040-1951(81)90165-7.

Bullen, M. E., D. W. Burbank, J. I. Gaver, and K. Y. Abdrakmatov (2001), Late Cenozoic tectonic evolution of the northwestern Tien Shan: New age estimates for the initiation of mountain building, *Geol. Soc. Am. Bull.*, *113*(12), 1544–1559, doi:10.1130/0016-7606(2001)113<1544:LCTEOT>2.0.CO;2.

Bullen, M. E., D. W. Burbank, and J. I. Garver (2003), Building the northern Tien Shan: Integrated thermal, structural, and topographic constraints, *J. Geol.*, *111*(2), 149–165, doi:10.1086/345840.

Burbank, D., A. Meigs, and N. Brozovic (1996), Interactions of growing folds and coeval depositional systems, *Basin Res.*, *8*(3), 199–223, doi:10.1046/j.1365-2117.1996.00181.x.

Burchfiel, B. C., E. T. Brown, D. Qidong, F. Xianyue, L. Jun, P. Molnar, S. Jianbang, W. Zhangming, and Y. Huichuan (1999), Crustal shortening on the margins of the Tien Shan, Xinjiang, China, *Int. Geol. Rev.*, *41*(8), 665–700, doi:10.1080/00206819909465164.

Burmeister, K. C., M. J. Harrison, S. Marshak, E. C. Ferré, R. A. Bannister, and K. P. Kodama (2009), Comparison of Fry strain ellipse and AMS ellipsoid trends to tectonic fabric trends in very low-strain sandstone of the Appalachian fold-thrust belt, *J. Struct. Geol.*, *31*, 1028–1038, doi:10.1016/j.jsg.2009.03.010.

Charreau, J., S. Gilder, Y. Chen, S. Dominguez, J. P. Avouac, S. Sen, M. Jolivet, Y. Li, and W. Wang (2006), Magnetostratigraphy of the Yaha section, Tarim Basin(China): 11 Ma acceleration in erosion and uplift of the Tian Shan mountains, *Geology*, *34*(3), 181–184, doi:10.1130/G22106.1.

Charreau, J., C. Gumiaux, J.-P. Avouac, R. Augier, Y. Chen, L. Barrier, S. Gilder, S. Dominguez, N. Charles, and Q. Wang (2009a), The Neogene Xiyu Formation, a diachronous prograding gravel wedge at front of the Tianshan: Climatic and tectonic implications, *Earth Planet. Sci. Lett.*, *287*, 298–310, doi:10.1016/j.epsl.2009.07.035.

Charreau, J., et al. (2009b), Neogene uplift of the Tianshan mountains observed in the magnetic record of the Jingou River section (northwest China), *Tectonics*, *28*, TC2008, doi:10.1029/2007TC002137.

Chen, J., D. W. Burbank, K. M. Scharer, E. Sobel, J. Yin, C. Rubin, and R. Zhao (2002), Magnetochronology of the Upper Cenozoic strata in the Southwestern Chinese Tian Shan: Rates of Pleistocene folding and thrusting, *Earth Planet. Sci. Lett.*, *195*(1–2), 113–130, doi:10.1016/S0012-821X(01)00579-9.

Chen, J., R. V. Heermance, D. W. Burbank, K. M. Scharer, J. Miao, and C. Wang (2007), Quantification of growth and lateral propagation of the Kashi anticline, southwest Chinese Tian Shan, *J. Geophys. Res.*, *112*, B03S16, doi:10.1029/2006JB004345.

Chen, J., B. Huang, and L. Sun (2010), New constraints to the onset of the India-Asia collision: Paleomagnetic reconnaissance on the Linzizong Group in the Lhasa Block, China, *Tectonophysics*, *489*(1–4), 189–209, doi:10.1016/j.tecto.2010.04.024.

Cifelli, F., M. Mattei, A. M. Hirt, and A. Günther (2004), The origin of tectonic fabrics in "undeformed" clays: The early stages of deformation in extensional sedimentary basins, *Geophys. Res. Lett.*, *31*, L09604, doi:10.1029/2004GL019609.

Du, Z., and Q. Wang (2007), Mesozoic and Cenozoic uplifting history of the Tianshan region: Insight from apatite fission track, *Dizhi Xuebao*, *81*(8), 1081–1101.

Dumitru, T. A., D. Zhou, E. Z. Chang, S. A. Graham, M. S. Hendrix, E. R. Sobel, and A. R. Carroll (2001), Uplift, exhumation, and deformation in the Chinese Tian Shan, *Mem. Geol. Soc. Am.*, *194*, 71–99, doi:10.1130/0-8137-1194-0.71.

Dunlop, D. J. (2002), Theory and application of the Day plot (M_{rs}/M_s versus H_{cr}/H_c): 1. Theoretical curves and tests using titanomagnetite data, *J. Geophys. Res.*, *107*(B3), 2056, doi:10.1029/2001JB000486.

Dunlop, D. J., and Ö. Özdemir (2001), *Rock Magnetism: Fundamentals and Frontiers*, 596 pp., Cambridge Univ. Press, Cambridge, U. K.

Evans, M. E., and F. Heller (2003), Enviromagnetic minerals, in *Environmental Magnetism: Principles and Applications of Enviromagnetics*, pp. 31–49, Academic, London.

Fu, B., A. Lin, K. Kano, T. Maruyama, and J. Guo (2003), Quaternary folding of the eastern Tian Shan, northwest China, *Tectonophysics*, *369*(1–2), 79–101, doi:10.1016/S0040-1951(03)00137-9.

Gilder, S., Y. Chen, and S. Sen (2001), Oligo-Miocene magnetostratigraphy and rock magnetism of the Xishuigou section, Subei (Gansu Province, western China), and implications for shallow inclinations in central Asia, *J. Geophys. Res.*, *106*(B12), 30,505–30,521, doi:10.1029/2001JB000325.

Heermance, R. V., J. Chen, D. W. Burbank, and C. Wang (2007), Chronology and tectonic controls of Late Tertiary deposition in the southwestern Tian Shan foreland, NW China, *Basin Res.*, *19*, 599–632, doi:10.1111/j.1365-2117.2007.00339.x.

Hendrix, M. S., S. A. Graham, A. R. Carroll, E. R. Sobel, C. L. McKnight, B. J. Schulein, and Z. Wang (1992), Sedimentary record and climatic implications of recurrent deformation in the Tian Shan: Evidence from Mesozoic strata of the north Tarim, south Junggar, and Turpan basins, northwest China, *Geol. Soc. Am. Bull.*, *104*(1), 53–79, doi:10.1130/0016-7606(1992)104<0053:SRACIO>2.3.CO;2.

Hendrix, M. S., T. A. Dumitru, and S. A. Graham (1994), Late Oligocene-early Miocene unroofing in the Chinese Tian Shan: An early effect of the India-Asia collision, *Geology*, *22*(6), 487–490, doi:10.1130/0091-7613(1994)022<0487:LOEMUI>2.3.CO;2.

Hrouda, F. (1982), Magnetic anisotropy of rocks and its application in geology and geophysics, *Geophys. Surv.*, *5*, 37–82, doi:10.1007/BF01450244.

Hrouda, F., and Š. Kahan (1991), The magnetic fabric relationship between sedimentary and basement nappes in the High Tatra Mountains, N. Slovakia, *J. Struct. Geol.*, *13*(4), 431–442, doi:10.1016/0191-8141(91)90016-C.

Huang, B., J. Piper, S. Peng, T. Liu, Z. Li, Q. Wang, and R. Zhu (2006), Magnetostragraphic study of the Kuche Depression, Tarim Basin, and Cenozoic uplift of the Tian Shan Range, western China, *Earth. Planet. Sci. Lett.*, *251*, 346–364, doi:10.1016/j.epsl.2006.09.020.

Huang, B., J. D. A. Piper, Q. Qiao, H. Wang, and C. Zhang (2010), Magnetostratigraphic and rock magnetic study of the Neogene upper Yaha section, Kuche Depression (Tarim Basin): Implications to formation of the Xiyu conglomerate formation, NW China, *J. Geophys. Res.*, *115*, B01101, doi:10.1029/2008JB006175.

Jackson, M. (1990), Diagentic sources of stable remanence in remagnetized Paleozoioc cratonic carbonates: A rock magnetic study, *J. Geophys. Res.*, *95*(B3), 2753–2761, doi:10.1029/JB095iB03p02753.

Jelinek, V. (1981), Characterization of the magnetic fabric of rocks, *Tectonophysics*, *79*(3–4), T63–T67, doi:10.1016/0040-1951(81)90110-4.

Ji, J., P. Luo, P. White, H. Jiang, L. Gao, and Z. Ding (2008), Episodic uplift of the Tianshan Mountains since the late Oligocene constrained by magnetostratigraphy of the Jingou River section, in the southern margin of the Junggar Basin, China, *J. Geophys. Res.*, *113*, B05102, doi:10.1029/2007JB005064.

Kligfield, R., W. Lowrie, A. Hirt, and A. W. B. Siddans (1983), Effect of progressive deformation on remanent magnetization of Permian redbeds from the Alpes Maritimes (France), *Tectonophysics*, *98*, 59–85, doi:10.1016/0040-1951(83)90211-1.

Larrasoaña, J. C., M. Gómez-Paccard, S. Giralt, and A. P. Roberts (2011), Rapid locking of tectonic magnetic fabrics in weakly deformed mudrocks, *Tectonophysics*, *507*, 16–25, doi:10.1016/j.tecto.2011.05.003.

Li, Y. (1984), *The Tertiary System of China*, 362 pp., Geol. Publ. House, Beijing.

Métivier, F., and Y. Gaudemer (1997), Mass transfer between eastern Tien Shan and adjacent basins (central Asia): Constraints on regional tectonics and topography, *Geophys. J. Int.*, *128*(1), 1–17, doi:10.1111/j.1365-246X.1997.tb04068.x.

Najman, Y., et al. (2010), Timing of India-Asia collision: Geological, biostratigraphic, and palaeomagnetic constraints, *J. Geophys. Res.*, *115*, B12416, doi:10.1029/2010JB007673.

Ogg, J. G., and A. G. Smith (2004), The geomagnetic polarity time scale, in *A Geological Time Scale 2004*, edited by F. Gradstein, J. Ogg, and A. Smith, pp. 63–86, Cambridge Univ. Press, Cambridge, U. K., doi:10.4095/215638.

Parés, J. M. (2004), How deformed are weakly deformed mudrocks? Insights from magnetic anisotropy, in *Magnetic Fabric: Methods and Applications*, edited by F. Martín-Hernández et al., *Geol. Soc. Spec. Publ.*, *238*, 191–203.

Parés, J. M., and B. A. van der Pluijm (2002), Evaluating magnetic lineations (AMS) in deformed rocks, *Tectonophysics*, *350*(4), 283–298, doi:10.1016/S0040-1951(02)00119-1.

Petrovský, E., and A. Kapička (2006), On determination of the Curie point from thermomagnetic curves, *J. Geophys. Res.*, *111*, B12S27, doi:10.1029/2006JB004507.

Reigber, C., G. W. Michel, R. Galas, D. Angermann, J. Klotz, J. Y. Chen, A. Papschev, R. Arslanov, V. E. Tzurkov, and M. C. Ishanov (2001), New space geodetic constrains on the distribution of deformation in central Asia, *Earth Planet. Sci. Lett.*, *191*, 157–165, doi:10.1016/S0012-821X(01)00414-9.

Reiners, P. W., and M. T. Brandon (2006), Using thermochronology to understand orogenic erosion, *Annu. Rev. Earth Planet. Sci.*, *34*(1), 419–466, doi:10.1146/annurev.earth.34.031405.125202.

Roberts, A. P., Y. Cui, and K. L. Verosub (1995), Wasp-waisted hysteresis loops: Mineral magnetic characteristics and discrimination of components in mixed magnetic systems, *J. Geophys. Res.*, *100*(B9), 17,909–17,924, doi:10.1029/95JB00672.

Sobel, E. R., and T. Dumitru (1997), Thrusting and exhumation around the margins of the western Tarim basin during the India-Asia collision, *J. Geophys. Res.*, *102*(B3), 5043–5063, doi:10.1029/96JB03267.

Sobel, E. R., J. Chen, and R. V. Heermance (2006), Late Oligocene–Early Miocene initiation of shortening in the southwestern Chinese Tian Shan: Implications for Neogene shortening rate variations, *Earth Planet. Sci. Lett.*, *247*(1–2), 70–81, doi:10.1016/j.epsl.2006.03.048.

Soto, R., J. C. Larrasoaña, L. E. Arlegui, E. Beamud, B. Oliva-Urcia, and J. L. Simón (2009), Reliability of magnetic fabric of weakly deformed mudrocks as a palaeostress indicator in compressive settings, *J. Struct. Geol.*, *31*(5), 512–522, doi:10.1016/j.jsg.2009.03.006.

Sun, J., and Z. Zhang (2009), Syntectonic growth strata and implications for late Cenozoic tectonic uplift in the northern Tian Shan, China, *Tectonophysics*, *463*(1–4), 60–68, doi:10.1016/j.tecto.2008.09.008.

Sun, J., Y. Li, Z. Zhang, and B. Fu (2009), Magnetostratigraphic data on Neogene growth folding in the foreland basin of the southern Tianshan Mountains, *Geology*, *37*(11), 1051–1054, doi:10.1130/G30278A.1.

Suppe, J., G. T. Chou, and S. C. Hook (1992), Rates of folding and faulting determined from growth strata, in *Thrust Tectonics*, edited by K. R. McClay, pp. 105–121, Chapman and Hall, London.

Tang, Z., Z. Ding, P. D. White, X. Dong, J. Ji, H. Jiang, P. Luo, and X. Wang (2011), Late Cenozoic central Asian drying inferred from a palynological record from the northern Tian Shan, *Earth Planet. Sci. Lett.*, *302*, 439–447, doi:10.1016/j.epsl.2010.12.042.

Tarling, D. H., and F. Hrouda (1993), *Magnetic Anisotropy of Rocks*, 573 pp., Chapman and Hall, London.

Tauxe, L. (2005), Applied rock (environmental) magnetism, in *Lectures in Paleomagnetism* [online], edited by L. Tauxe, Univ. of Calif. Press, Berkeley. [Available at http://earthref.org/MAGIC/books/Tauxe/2005/]

Tauxe, L., T. A. T. Mullender, and T. Pick (1996), Potbellies, wasp-waists, and superparamagnetism in magnetic hysteresis, *J. Geophys. Res.*, *101*(B1), 571–583, doi:10.1029/95JB03041.

Weil, A. B., and A. Yonkee (2009), Anisotropy of magnetic susceptibility in weakly deformed red beds from the Wyoming salient, Sevier thrust belt: Relations to layer-parallel shortening and orogenic curvature, *Lithosphere*, *1*(4), 235–256, doi:10.1130/L42.1.

Willett, S. D., and M. T. Brandon (2002), On steady states in mountain belts, *Geology*, *30*(2), 175–178, doi:10.1130/0091-7613(2002)030<0175:OSSIMB>2.0.CO;2.

Windley, B. F., M. B. Allen, C. Zhang, Z. Y. Zhao, and G. R. Wang (1990), Paleozoic accretion and Cenozoic redeformation of the Chinese Tien Shan Range, central Asia, *Geology*, *18*(2), 128–131, doi:10.1130/0091-7613(1990)018<0128:PAACRO>2.3.CO;2.

Woodcock, N. H. (1977), Specification of fabric shapes using an eigenvalue method, *Geol. Soc. Am. Bull.*, *88*(9), 1231–1236, doi:10.1130/0016-7606(1977)88<1231:SOFSUA>2.0.CO;2.

Xinjiang Institute of Geography (1986), *The Evolution of the Tian Shan* [in Chinese], 188 pp., Sci. Press, Beijing.

Yang, Y., and M. Liu (2002), Cenozoic deformation of the Tarim plate and the implications for mountain building in the Tibetan Plateau and the Tian Shan, *Tectonics*, *21*(6), 1059, doi:10.1029/2001TC001300.

Yi, Z., B. Huang, J. Chen, L. Chen, and H. Wang (2011), Paleomagnetism of early Paleogene marine sediments in southern Tibet, China: Implications to onset of the India–Asia collision and size of Greater India, *Earth Planet. Sci. Lett.*, *309*, 153–165, doi:10.1016/j.epsl.2011.07.001.

Yin, A., S. Nie, P. Craig, T. M. Harrison, F. J. Ryerson, X. Qian, and G. Yang (1998), Late Cenozoic tectonics evolution of the southern Chinese Tian Shan, *Tectonics*, *17*(1), 1–27, doi:10.1029/97TC03140.